ACS OMEGA

http://pubs.acs.org/journal/acsodf
Article

Molecular Precursor Approach to Sulfur-Free $CuInSe_2$: Replacing Thiol Coordination in Soluble Metal Complexes

Jonathan W. Turnley, Swapnil D. Deshmukh, Victoria M. Boulos, Ryan G. Ellis, Nicole J. LiBretto, Judy Kuan-Yu Liu, Jeffrey T. Miller, Hilkka I. Kenttämaa, and Rakesh Agrawal*

Cite This: *ACS Omega* 2023, 8, 47262−47270
Read Online

ACCESS | Metrics & More | Article Recommendations | Supporting Information

ABSTRACT: Solution-processed $CuInSe_2$ films have generally relied on sulfide or sulfoselenide precursor films that, during the grain growth process, hamper the growth of thicker films and lead to the formation of a fine-grain layer. However, recent research has indicated that sulfur reduction in the precursor film modifies the grain growth mechanism and may enable the fabrication of thicker absorbers that are free of any fine-grain layer. In this work, we pursue direct solution deposition of sulfur-free $CuInSe_2$ films from the molecular precursor approach. To this end, we tune the amine−thiol reactive solvent system and study the changes to the resulting soluble complexes through a combination of analytical techniques. We show that by reactively dissolving indium(III) selenide and selenium in solutions of *n*-butylamine and 1,2-ethanedithiol, a metal thiolate species is formed, and that this metal thiolate can be modified by isolation from the thiol-containing solvent via precipitation. As the quantity of selenium in the ink increases, the thiol content in the complex decreases, eventually producing soluble $[InSe_x]^-$ species. Extending this method to be used with copper selenide as a copper source, molecular precursor inks can be made for solution-processed, sulfur-free $CuInSe_2$ films. We then show that these $CuInSe_2$ precursor films can be fully coarsened without a fine-grain layer formation, even at the desired thicknesses of 2 μm and greater.

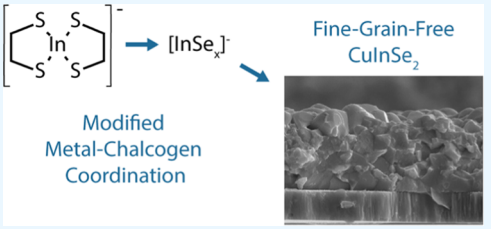

INTRODUCTION

The $Cu(In,Ga)(S,Se)_2$ family of semiconducting materials has seen broad application in the field of photovoltaics (PV). Single-junction solar cells with efficiencies above 23% have been made with a $Cu(In,Ga)Se_2$ absorber.[1] On the other hand, $CuInSe_2$, with its band gap of around 1 eV, has been used as the bottom cell in tandem photovoltaics.[2] While the highest efficiency devices have been made with vacuum deposition, this material system can also be solution-deposited. Solution processing offers great promise in reducing the cost to manufacture PV panels while simultaneously increasing throughput, maintaining large-area uniformity, and improving material utilization.[3,4]

Vacuum deposition of these materials is often performed via coevaporation, where the selenide semiconductor is either directly deposited or made by heating a metal stack in a selenium-containing atmosphere.[5,6] In contrast, solution processing has generally started with a sulfide or sulfoselenide film that is later converted to the desired selenide material by heating in a selenium-containing atmosphere (referred to as selenization) after Guo et al. had success with this method in 2009.[7−11] Clark et al. have pointed out that developing a method to directly solution deposit the pure selenide $CuInSe_2$ or $Cu(In,Ga)Se_2$ could simplify the fabrication process and make it easier to scale up solution processing methods.[12] Additionally, the composition of the precursor material is likely connected to the morphology of the final coarse-grain absorber. Specifically, the conversion of the sulfide precursor to a selenide material may contribute to the formation of the notorious fine-grain layer that has generally plagued solution-processed $Cu(In,Ga)(S,Se)_2$ solar cells, especially with absorber layers thicker than 1 μm.[8] While carbonaceous impurities have often been blamed for the formation of this layer, it has also been shown that even when the carbon is removed, a small fine-grain layer persists.[13] Deshmukh et al. built upon this observation and showed that increasing the selenium content in $CuIn(S,Se)_2$ precursor films can alter the grain growth mechanism and prevent the formation of the fine-grain layer.[14]

Solution processing methods can broadly be classified by the form of the precursors in the coating inks: colloidal nanoparticles and molecular precursors.[3] Colloidal nanoparticle inks of $CuInSe_2$ have been used to directly coat sulfur-free precursors.[15] However, the nanoparticles are generally stabilized in the colloid with the use of large carbonaceous surface ligands. During the process of coating and heat-treating films from these nanoparticles, the ligands

Received: September 28, 2023
Accepted: November 13, 2023
Published: December 1, 2023

can decompose into inorganic carbon that remains in the film as a contaminant and limits further processing.[8] Ligand exchange methods can be used to replace large organic ligands with small inorganic ligands, but this adds additional process complexity.[13] Direct synthesis of nanoparticles with small inorganic ligands is also possible but has yet to lead to high device efficiencies.[16] A molecular precursor approach could bypass these limitations and eliminate carbonaceous residues by tuning the decomposition of the soluble complexes.

Metal organics based on selenolates have been used as single-source and dual-source precursors for solution-processed $CuInSe_2$.[17,18] Similarly, Dhingra et al. utilized molecular precursor inks containing the soluble metal polyselenides $(Ph_4P)_2[Cu_4Se_{12}]$ and $(Et_4N)_3[In_3Se_{15}]$ to directly deposit $CuInSe_2$ films.[19] However, the complex synthesis of these metal organics and metal polyselenides could be prohibitive for scale-up, and the large organic structures in these species could introduce carbonaceous impurities in the film. Clark et al. deposited $CuInSe_2$ films with inks containing CuCl, $InCl_3$, and $SeCl_4$ in dimethylformamide.[12] However, they found that the volatility of $InCl_3$ posed a major issue in maintaining an appropriate stoichiometry as it would begin to leave the film before it could react with the selenium source during the needed annealing step. Diorganyl diselenides have been used as an external selenium source instead of $SeCl_4$ for $CuInSe_2$ nanoparticles, but in the context of direct molecular precursor deposition, this still leaves the challenge of finding appropriate metal precursors.[20,21]

One promising route to overcome these limitations is with the amine−thiol reactive solvent system. Various combinations of amine and thiol solutions can dissolve a wide range of metal salts, metal chalcogenides, metals, and chalcogens.[22−25] In the case of metals, dissolution occurs because of the formation of metal thiolates, which are then soluble in the amine. Subsequently, these metal thiolates can decompose into metal sulfides upon heating.[9] The reactive dissolution of metal selenides and selenium opens the possibility for including selenium into the solution-processed films.[26] However, the thiols in the ink can still act at a sulfur source.[27] This means that for the same ink, the sulfur-to-selenium ratio in the resulting material may be dictated by the reaction conditions. In fact, it has recently been reported that even when using an amine−thiol ink containing Cu_2Se, In_2Se_3, and excess selenium, the resulting material contained sulfur in the crystal structure and was therefore $CuIn(S,Se)_2$ rather than the targeted $CuInSe_2$.[14] Therefore, the chemistry and decomposition of these soluble precursors must be carefully tuned to produce sulfur-free $CuInSe_2$ films.

In this work, we have studied the soluble complexes formed upon reactive dissolution of metal selenides in monoamine−dithiol mixtures. Analysis through a combination of Raman spectroscopy, X-ray absorption spectroscopy, inductively coupled plasma optical emission spectroscopy, X-ray fluorescence, and electrospray ionization mass spectrometry has shown that while direct dissolution of indium(III) selenide in butylamine−ethanedithiol solutions forms an indium thiolate, the indium complex can be altered by the addition of excess selenium and the separation from bulk thiol. These new soluble complexes are free of thiol and contain indium−selenium bonding. Extending these methods for copper selenide, we then utilize these precursors to fabricate sulfur-free $CuInSe_2$ films through the molecular precursor method with the desired composition and little-to-no carbonaceous residue. Finally, we confirm our recent finding on the role of precursor composition on the final film morphology by showing that a 2 μm selenide precursor film can be fully coarsened with no fine-grain layer.[14]

EXPERIMENTAL SECTION

Materials. Selenium powder (99.99%), selenium pellets (99.995%), copper nanopowder (99.5%, 60−80 nm), copper(I) selenide (99.95%), *n*-butylamine (BA) (99.5%), zinc sulfate heptahydrate (99.995%), 1,2-ethanedithiol (EDT) (98%), toluene (anhydrous, 99.8%), cyclohexane (anhydrous, 99.5%), and *n*-methyl-2-pyrrolidone (NMP) (anhydrous, 99.5%), were purchased from Sigma-Aldrich. Trace-metal grade nitric acid, indium (99.999%), and indium(III) selenide (99.99%) were purchased from Fisher. All materials were used as received without further purification. Nitric acid was stored in air, and all other chemicals were stored in a glovebox under a nitrogen atmosphere. The crystal structure of the as-purchased Cu_2Se and In_2Se_3 was investigated by X-ray diffraction (Figures S1 and S2).

Preparation and Isolation of Complexes. All preparations of amine−thiol-based complexes were performed in a glovebox under a nitrogen atmosphere. The indium precursor was dissolved overnight on a heated stir plate at 35 °C in a BA-EDT solution at an In/BA/EDT mole ratio of 1:8:4, with the addition of selenium for specified samples. As a control, treatment 1 (T1) used indium metal as the precursor, with no additional selenium. In treatment 2 (T2), indium(III) selenide was used, with no additional selenium. For treatment 3 (T3) and treatment 4 (T4), indium(III) selenide and additional selenium were used at Se/In_2Se_3 ratios of 3:1 and 6:1, respectively. In this study, the complexes formed in the amine−thiol dissolution were isolated from the amine−thiol and redissolved in NMP. The isolation of the complexes was performed via precipitation and centrifugation. Briefly, between 200 and 500 μL of reacted amine−thiol solution was combined with 20 mL of toluene and 1 mL of cyclohexane, which resulted in precipitation of solids from the solution. The solid was isolated via centrifugation at 14,000 rpm for 5 min, followed by decanting of the supernatant and drying under vacuum for 2 min. The complex was further purified by redissolution and repeating the isolation steps. The dried complex was redissolved in 100−200 μL of *n*-butylamine. The complex was again isolated by the same procedure with an additional 15 min of drying. To make an ink for coating $CuInSe_2$ films, complexes were isolated from a T3 sample as described above. Additionally, Cu_2Se + Se was dissolved at the same metal/BA/EDT ratio as listed above and isolated by the same procedure. The isolated complexes were redissolved in NMP at a nominal metal concentration of approximately 0.4 M. The solutions were then combined, resulting in an ink (referred to as the CISe ink) with a Cu/In ratio of approximately 0.8. The ink was coated via automated doctor blading on a heated stage to a thickness of approximately 2 μm. The film was then selenized at 540 °C for 20 min in a tube furnace with selenium pellets. For comparison, a conventional amine−thiol ink was made (referred to as the CIS ink) by dissolving copper(I) sulfide and indium in BA + EDT. The film was then selenized at 500 °C for 25 min.[14]

Characterization. Raman spectroscopy was performed by using a Horiba/Jobin-Yvon HR800 Raman spectrometer with a 632.8 nm excitation laser wavelength. For the collection of spectra on liquid solutions or the isolated complexes, the

https://doi.org/10.1021/acsomega.3c07515
ACS Omega 2023, 8, 47262−47270

samples were kept in a quartz cuvette enclosed in a nitrogen atmosphere. Electrospray ionization high-resolution tandem mass spectrometry (ESI-MS/MS) samples were characterized by using a Thermo Scientific LTQ Orbitrap XL hybrid mass spectrometer equipped with an electrospray ionization (ESI) source. The solutions were infused into the ESI source at a rate of 5−7 μL min^{-1} using a syringe pump. The ESI source conditions were set to the following: 3 kV spray voltage, 40 (arbitrary units) flow rate of sheath gas (N_2), 10 (arbitrary units) flow rate of auxiliary gas (N_2), and 275 °C capillary temperature. Voltages for the ion optics were optimized by using the tuning features of the LTQ Tune Plus interface. Mass spectra were collected in both negative- and positive-ion modes. Elemental compositions were obtained via high-resolution mass analysis and were further confirmed based on isotopic distribution patterns and collision-activated-dissociation (CAD) mass spectra. CAD experiments involved the isolation of ions of a selected m/z value such that only ions of the same nominal m/z value were isolated in the ion trap, kinetically excited, and subsequently allowed to collide with helium buffer gas always present in the trap. The collisions caused the ions to fragment and, thus, allowed for their structural identification. Representative CAD mass spectra are shown in Figures S3−S8. Samples were prepared under a nitrogen atmosphere to minimize potential exposure to oxygen and moisture. Inductively coupled plasma optical emission spectroscopy (ICP-OES) was performed with an iCAP 7400 ICP-OES analyzer after digestion in trace-element nitric acid. For proper sulfur analysis, microwave digestion was utilized at a temperature of 180 °C. Standards were made by dissolving the respective elements in nitric acid and diluting with ultrapure water, except for sulfur analysis, which used zinc sulfate heptahydrate in ultrapure water as the sulfur standard. In situ XAS experiments were performed at beamline 10-ID at the Advanced Photon Source (APS) at Argonne National Laboratory. Measurements were performed at the In K-edge (27.940 keV) in transmission mode using a fast scan from 250 eV below the edge to 550 eV above the edge, which took approximately 10 min per scan. In-edge samples were prepared at a 0.5 M In concentration in solution. All samples were sealed in a liquid sample cell in an air-free atmosphere. Standard fitting procedures were used to fit the extended X-ray absorption fine structure (EXAFS). The intrinsic loss factor S_0^2 was calibrated by fitting the foil and found to be 0.71 at the Cu edge and 0.8 at the In edge. Least-squares fits for the first shell of r space and isolated q space were performed on the k^2-weighted Fourier transform (FT) data over the range 2.7−10 Å^{-1} in each spectrum to fit the magnitude and imaginary components. In−S (CN = 1; R = 2.45 Å) and In−Se (CN = 1; R = 2.60 Å) scattering pairs were considered using FEFF6 calculations. The error in the coordination number (CN) calculation is ±10%, and the error in the bond distance is ±0.01 Å.

RESULTS AND DISCUSSION

Preparation and Isolation of Complexes. Indium metal, indium(III) selenide, and selenium are all known to dissolve in monoamine−dithiol solutions. Studies on the dissolution of indium metal in these solutions of monoamine and 1,2-ethanedithiol (EDT) have identified the formation of bis(1,2-ethanedithiolate) indium(III) that is charge balanced by an n-alkylammonium.[9] Furthermore, it was shown that this species could be isolated by evaporation of the bulk solvent. Studies on the dissolution of selenium in solutions of monoamines and diamines with monothiol have shown that selenium can take various forms, including forming polyselenide ions and binding to the thiolate.[28,29] Our analysis indicates that similar polyselenide ions may also be formed in the presence of dithiol, as evidenced through Raman spectroscopy by the presence of a peak just below 250 cm^{-1} that corresponds to Se−Se bonding (see Figure S9). While much work has been done to understand the chemistry behind the amine−thiol reactive solvent system, there are still several gaps of knowledge that this work seeks to address. First, further work is needed to better understand the complexes that arise from the reaction of metal chalcogenides like indium(III) selenide in amine−thiol solutions. In particular, it is important to analyze key structural aspects of these complexes, such as the presence and type of metal chalcogen bonding as this can impact their use as precursors for metal chalcogenides. Second, more complex, multinary chalcogenide, amine−thiol inks are often used to provide multiple precursors simultaneously. But, further work is needed to understand how different complexes may interact with each other in these amine−thiol solutions. Finally, modifications to the amine−thiol solvent system are needed to better control the chalcogen content in the resulting thin films, particularly when sulfur-free metal selenides are desired.

Given that the thiols can act as a sulfur source, we sought to remove the soluble complexes from the bulk thiol-containing solvent. While soluble complexes were previously isolated from amine−thiol solutions by evaporation, we found isolation via precipitation to be quick and effective. Upon addition of an excess of toluene and cyclohexane as miscible nonpolar antisolvents, solid formation is immediately observed. These complexes are then easily isolated by centrifuging and decanting the supernatant. The complexes from solutions made with indium and indium selenide could then be redissolved in n-butylamine (BA) or other polar solvents, such as n-methyl-2-pyrrolidone (NMP), dimethyl sulfoxide, or dimethylformamide. In this study, each of the treatments refers to different precursors that are dissolved in BA-EDT solutions and subsequently isolated via precipitation. The precursors are In, In_2Se_3, In_2Se_3 + 3Se, and In_2Se_3 + 6Se for T1, T2, T3, and T4, respectively.

Raman Analysis of Isolated Complexes. T1 provides a convenient reference for this investigation with a simple, known structure of bis(1,2-ethanedithiolate) indium(III) that forms upon the dissolution of indium metal in butylamine−ethanedithiol solutions.[9] Raman analysis (Figure 1) of the isolated complexes can be used to identify the bonding within the various species. In T1, the peaks in the region of 150−350 cm^{-1} are expected to be attributed to various vibrations of the In−S bonds.[30,31] For T2, which utilized In_2Se_3 rather than indium metal, the spectrum shares some peaks with the T1 spectrum, implying that In−S bonding could be present in the complex. Peak assignment is complicated as changes in the local environment could change the vibrational energies of the In−S bonds leading to peak shifts. However, there is also a new strong peak at approximately 173 cm^{-1}. Based on previous Raman analysis of hydrazine-based indium−selenium complexes, we can attribute this peak to the presence of In−Se bonding in the complex.[31,32] For T3, utilizing In_2Se_3 + 3Se as the precursor, we see further changes in the Raman spectrum, and peaks associated with In−S bonding are no longer present in the sample.

https://doi.org/10.1021/acsomega.3c07515
ACS Omega 2023, 8, 47262−47270

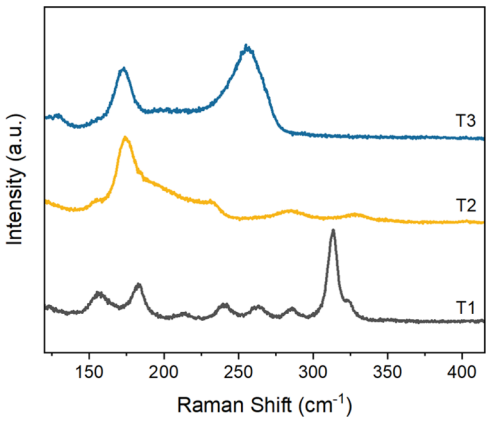

Figure 1. Raman spectra for the isolated complexes from T1 (with In as the precursor), T2 (with In_2Se_3 as the precursor), and T3 (with In_2Se_3 + 3Se as the precursor).

The In−Se bonding peak at 173 cm^{-1} remains and is accompanied by a peak at 257 cm^{-1} that can be attributed to the presence of Se−Se bonding.[29] This suggests that after isolation, the coordination around the indium in T3 has changed compared to that of the indium thiolate in T1, though further characterization is needed to develop a more detailed understanding of the new structures. While T3 uses the precursors of In_2Se_3 + 3Se, we found that the same Raman spectrum could be obtained from the isolated complex while using indium metal and elemental selenium at the same In/Se mol ratio of 1:3 (see Figure S10).

XAS Analysis of Complexes Before and After Isolation. While the changes in the indium precursor clearly affect the structure of the precipitated complex, particularly in the presence of excess selenium, the role of the isolation process itself is unclear from the Raman data alone. Synchrotron-based X-ray absorption spectroscopy (XAS) was used to investigate the oxidation state and bonding environment of indium in the complex from T3 before and after precipitation. X-ray absorption near-edge spectroscopy (XANES) (Figure 2a) shows a consistent edge energy of 27.9431 keV for samples before precipitation (in a BA-EDT solution) and after precipitation (in an NMP solution). This value is consistent with previous reports on bis(1,2-ethanedithiolate) indium(III) and indicates that indium is in an oxidation state of +3 before and after isolation.[9] On the other hand, the extended X-ray absorption fine structure (EXAFS) (Figure 2b) shows that the indium in the post-isolation sample has more first-shell neighbors at a longer bond distance than the pre-isolation sample. A summary of the structural parameters obtained from the best fit to the EXAFS data is listed in Table 1. The preisolation sample contains 4 In−S bonds at 2.45 Å, which closely matches the structure of bis(1,2-ethanedithiolate) indium(III). After precipitation and redissolution in NMP, bond distance elongation was observed with a simultaneous increase in coordination number, consistent with In−Se scattering. Therefore, during the isolation step, a distinct structural change in the indium complex was observed. This result is consistent with Raman analysis, which also suggested that indium was bonded to selenium following isolation. However, it provides new insight that before isolation, when still dissolved in the amine−thiol solution, the indium is bonded to sulfur. This means that the transformation from In−S bonding to In−Se bonding occurs

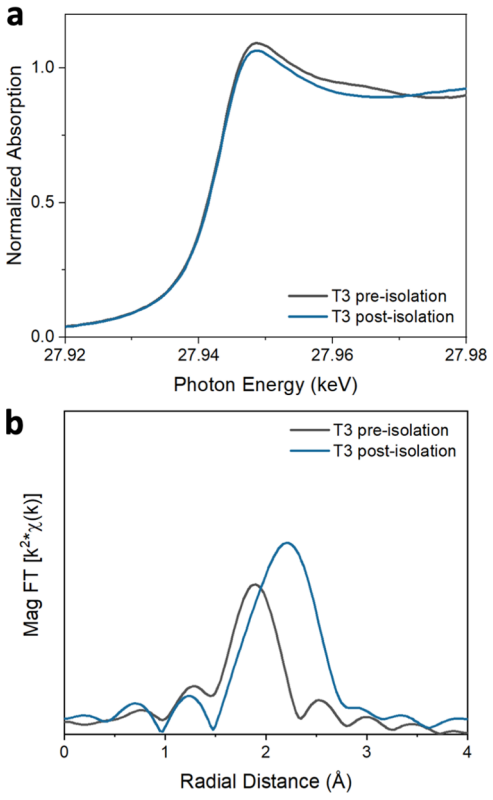

Figure 2. (a) Indium-edge XANES and (b) EXAFS of T3 before isolation (in a BA-EDT solution) and after isolation (in an NMP solution).

Table 1. Structural Parameters from Best Fit of Spectra at In K-Edge

sample	XANES energy (keV)	scattering pair	CN	R (Å)	σ^2	E_0 (eV)
T3 pre-isolation	27.9431	In−S	4.0	2.45	0.006	−1.4
T3 post-isolation	27.9431	In−Se	6.0	2.58	0.006	3.2

during the isolation process. We hypothesize that the presence of free thiol in the pre-isolation solution may play a role in an equilibrium, favoring the formation of bis(1,2-ethanedithiolate) indium(III). However, when thiol is removed, there is a shift in the equilibrium toward a complex where indium is bound to selenium.

ICP-OES Analysis of Isolated Complexes. To further our understanding of the elemental composition of these complexes and to confirm that sulfur is being removed during the isolation process, we investigated elemental analysis with ICP-OES (Table 2). For T1, the expected bis(1,2-ethanedithiolate) indium(III) species with a chemical formula of $[In(SCH_2CH_2S)_2]^-$ would have 4 sulfurs per indium, which is

Table 2. Compositional Analysis of Isolated Complexes via ICP-OES

treatment	precursor	S/In mol ratio	Se/In mol ratio
T1	In	3.9	7.8×10^{-4}
T2	In_2Se_3	0.78	1.7
T3	In_2Se_3 + 3Se	0.095	3.3
T4	In_2Se_3 + 6Se	0.010	4.9

https://doi.org/10.1021/acsomega.3c07515
ACS Omega 2023, 8, 47262−47270

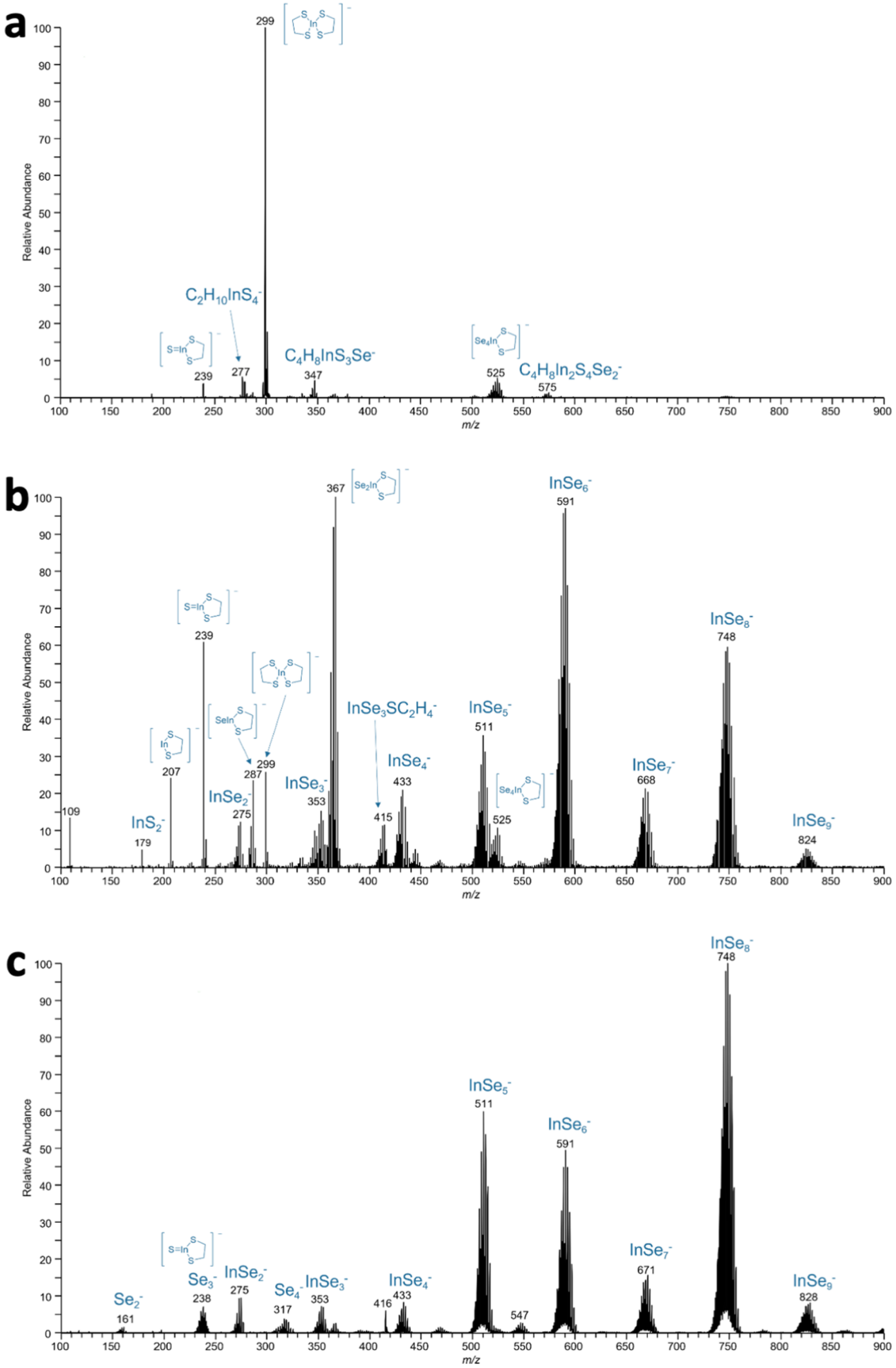

Figure 3. Negative-ion mode ESI mass spectra of butylamine solutions containing the isolated complexes from (a) T2, (b) T3, and (c) T4.

https://doi.org/10.1021/acsomega.3c07515
ACS Omega 2023, 8, 47262−47270

in agreement with 3.9 measured by ICP-OES. Interestingly, that value drops to less than 1 sulfur per indium for T2. This observation makes sense as indium metal will not dissolve with less than 2 EDT per indium, but In_2Se_3 will dissolve at a lower dithiol-to-indium ratio. During isolation, the complex could be driven to the stable species with the minimum number of dithiols incorporated. By introducing elemental selenium as a precursor in T3 and T4, we can effectively remove the remaining sulfur from the complex. For the case of T4, no sulfur was detected above the level of the blank. This trend is confirmed through observations with X-ray fluorescence (XRF) as shown in Figure S11. This reduction in sulfur indicates that not only is the thiol no longer bound to the indium but it is fully removed from the complex. Interestingly, the Se/In ratio is greater than expected if all indium and selenium were retained through the precipitation. This indicates that during the isolation of the complex, indium is preferentially lost. We hypothesize that this may be the result of the indium thiolate having a slight solubility in the nonpolar antisolvent.

ESI-MS Analysis of Isolated Complexes. ESI-MS was used to better understand the structure of the complexes by studying the mass/charge ratios of the constituent ions and fragmentation products. Previous work on the dissolution of indium metal in monoamine−ethanedithiol solutions (used as T1 in this study) identified peaks at m/z 299 and 239 in negative-ion mode corresponding to bis(1,2-ethanedithiolate) indium(III) and a fragmentation product of bis(1,2-ethanedithiolate) indium(III), respectively.[9] Investigation of the complex formed in T2 (Figure 3a) similarly shows a peak at m/z 299 in negative mode that corresponds to bis(1,2-ethanedithiolate) indium(III). However, based on elemental analysis via ICP-OES, the low sulfur-to-indium ratio of 0.78 indicates that this cannot be the primary compound. Not every analyte will respond to ionization in the same way; thus, the relative intensities of various species in ESI-MS are not necessarily quantitative. Previous work with similar metal thiolates suggests that they are highly ionizable, so it is reasonable to expect that metal thiolates could be over-represented in an ESI-MS spectrum relative to other metal complexes in the samples.[33] Interestingly, we also observe the presence of ions that contain indium, selenium, and thiolates at m/z values of 347, 525, and 575. Similar species may exist in a form that provides the previously identified stoichiometry but are difficult to ionize and therefore not easily detected by this method. For T3, the negative mode ESI-MS (Figure 3b) shows a mixture of indium-containing ions with thiolates, selenium, or both thiolates and selenium present. Based on ICP-OES and XRF analyses, there is very little sulfur present in the isolated complexes from T3, so we can presume that the ions containing only indium and selenium are dominant. Further work is needed to better understand the structure of these indium- and selenium-containing ions. However, given the large ratio of selenium to indium in $InSe^{5-}$, $InSe^{6-}$, $InSe^{7-}$, and $InSe^{8-}$ species, it is likely that polyselenide chains or rings are present. This idea is further supported by the Se−Se bonding observed with Raman spectroscopy. Polyselenide chains and rings are known in the literature to take the form Se_x^{2-}, where x can generally range from 2 to 8.[34] The presence of ions containing indium and polyselenides harkens back to work done by the Kanatzidis group, who made a number of soluble indium polyselenide species, generally utilizing polyselenide chains of $x = 4$ or $x = 5$. Interestingly, they had larger selenium to indium ratios of 5 and 10.5, whereas our T3 sample has a ratio of 3.3.[35,36] The negative mode ESI-MS of sample T4 (Figure 3c) primarily shows the presence of indium- and selenium-containing ions. The only detection of thiolate species comes in the form of the fragmented bis(1,2-ethanedithiolate) indium(III) peak at m/z 238, which in this spectra overlaps with the presence of polyselenide ions of chain length equal to 3. Both of these isobaric peaks were differentiated and confirmed by utilizing high-resolution and CAD ESI-MS/MS experiments (Figure S5). The presence of free polyselenide ions was not observed for T3. Positive-mode ESI-MS (Figures S12−S14) for all samples showed peaks that correspond to the ionization of butylamine solvent. Based on research into amine−thiol dissolutions of indium, we similarly expect that the most likely cation in each of these complexes would be *n*-butylammonium.[9] While this matches the ESI-MS observations, this result is complicated in that the samples are run with butylamine as the bulk solvent, which would produce the same species upon ionization. However, no evidence of other cations besides *n*-butylammonium was observed.

Application to Sulfur-Free $CuInSe_2$. The ability to create soluble indium- and selenium-containing complexes that are free of sulfur is an exciting result in the pursuit of solution-deposited $CuInSe_2$ films. Copper(I) selenide is soluble via reactive dissolution in amine−thiol, so the same methods were applied to this system. The isolated Cu-containing species lacked solubility in amine when compared to the indium-containing species previously investigated. Additionally, differences in the efficiency of sulfur removal were observed in ICP-OES (Table 3). When Cu metal is used as the precursor, a sulfur-to-copper ratio of 1.2 was observed after isolation. This value is consistent with the 1.2 sulfurs per copper in the copper−ethanedithiolate cluster observed by Zhao et al. when using this amine−thiol chemistry.[9] As observed with the indium precursors, switching from a Cu metal precursor to a Cu_2Se precursor resulted in less sulfur being retained in the isolated complex. However, unlike with the indium precursors, adding more selenium did not reduce the sulfur content further. In fact, additional sulfur may be retained, possibly through an interaction between the selenium and the thiol, similar to what was observed by Deshmukh et al.[29]

Table 3. Compositional Analysis of Isolated Copper Complexes via ICP-OES

precursor	S/Cu mol ratio	Se/Cu mol ratio
Cu	1.2	6.4×10^{-4}
Cu_2Se	0.31	0.41
Cu_2Se + Se	0.51	0.77
Cu_2Se + 3Se	0.40	1.4

Despite the limitations of the copper source, the complex could be dispersed in NMP as a slurry and combined with the soluble indium source for a combined ink. Isolated samples from Cu_2Se + Se were combined with the complex obtained from In_2Se_3 + 3Se and then used to make a thin film via automated blade coating and annealing. XRD analysis of this precursor film (termed the CISe precursor film) confirmed the formation of chalcopyrite $CuInSe_2$ (Figure 4a). However, a small amount of sulfur in the crystal lattice could be difficult to identify by this method.

Raman spectroscopy was employed to validate the formation of $CuInSe_2$ and also to check for sulfur-related vibrations that

https://doi.org/10.1021/acsomega.3c07515
ACS Omega 2023, 8, 47262−47270

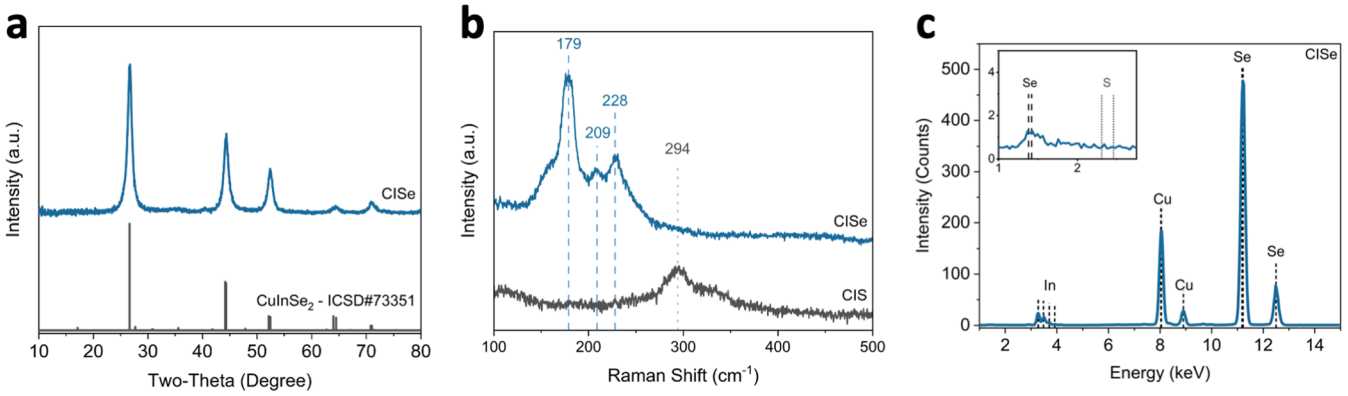

Figure 4. (a) XRD pattern obtained from the CISe precursor fabricated from the molecular precursor ink containing the metal−selenium complexes, (b) the Raman spectrum of the CISe precursor film compared to a CIS film fabricated from metal−thiolates, and (c) the XRF spectrum from the CISe precursor material with an inset focused on the region where sulfur peaks would appear.

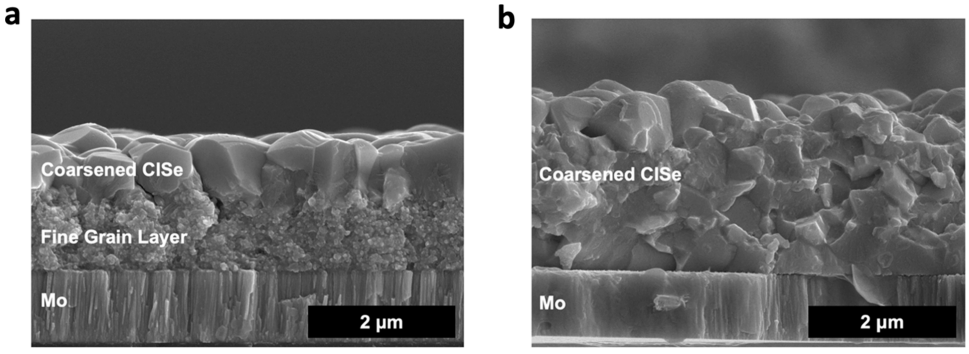

Figure 5. SEM images showing grain growth after selenization of (a) a sulfide CIS precursor film and (b) a selenide CISe precursor film.

would indicate an alloyed $CuIn(S,Se)_2$ material (Figure 4b). The A_1 mode vibration in $CuIn(S,Se)_2$ originates from the vibrations of the anions in the crystal structure.[37] The corresponding peak in Raman spectroscopy will appear around 174 cm^{-1} for selenium-related vibrations and around 290 cm^{-1} for sulfur-related vibrations, though the exact location of each peak can be shifted by changes in the surrounding atoms and the presence of defects.[37−39] The CISe precursor film from the new metal−selenium-containing ink was compared to a film made from a traditional ink-containing copper thiolates and indium thiolates (referred to as the CIS precursor film). While the CIS film shows the formation of $CuInS_2$ with the observed A_1 peak at 294 cm^{-1}, the CISe precursor film confirmed the presence of $CuInSe_2$ through the Raman peak observed at 179 cm^{-1} (Figure 4). Additionally, the peaks observed at 209 and 228 cm^{-1} can be attributed to the B_2/E vibration modes of $CuInSe_2$. The shoulder observed off of the A_1 peak in the CISe sample may signify the presence of the ordered vacancy compounds, $CuIn_3Se_5$ or $CuIn_5Se_8$, which commonly forms on the surface of $CuInSe_2$ thin films and can play a beneficial role in solar cell performance.[40,41] Importantly, no evidence of sulfur in the film was observed, as Raman peaks in the region of 290 cm^{-1} were absent.

To further validate that the CISe precursor film was sulfur-free, the sample was analyzed by XRF (Figure 4c). Note that to provide clarification in the analysis, the material was scrapped off the molybdenum substrate as molybdenum and sulfur emission lines overlap. The XRF data qualitatively shows the presence of copper, indium, and selenium, but there is no evidence of sulfur. This again provides evidence for the formation of a sulfur-free $CuInSe_2$ precursor film.

An additional benefit of the precursors in this ink may be a reduction in carbon impurities in the film. In the Supporting Information, the full Raman spectra for the precursor films from the CIS and CISe precursor films are shown (Figure S15). The sulfide film shows large peaks in the range of 1300−1600 cm^{-1} that indicate the presence of carbon−carbon bonding.[42] However, for the selenide film, these peaks are dramatically reduced. The presence of a carbonaceous residue in the sulfide CIS film may be due to the decomposition of the metal thiolates. By cleaving the C−S bond to produce the metal sulfides, a reactive carbon species is created, which could lead to the formation of a large carbon network.[43] However, as the metal−selenium complex from this investigation breaks down, rather than producing carbonaceous residue, excess selenium is produced, which can volatilize and leave the film during heat treatment.

For further use in solar cells, the nanocrystalline precursor film must undergo grain growth to produce a coarse-grain material. However, this grain growth process has long been hindered by the formation of an undesired fine-grain layer. While much work has connected this layer to carbon impurities,[8] more recently, the sulfide-to-selenide conversion has also been connected to fine-grain layer formation.[14] While vacuum-deposited $Cu(In,Ga)Se_2$ films are generally in excess of 2 μm, researchers utilizing solution-processed methods have generally been limited to around 1.2−1.3 μm to minimize the size of the fine-grain layer.[44] To emphasize this point, an SEM image is shown in Figure 5a of a coarse-grain film made by

https://doi.org/10.1021/acsomega.3c07515
ACS Omega 2023, 8, 47262−47270

selenizing a 2 μm sulfide $CuInS_2$ precursor film. It can clearly be seen that grain growth is limited to less than the top 1 μm of the film, with the rest of the film being composed of fine grains.

With these metal−selenium precursors, we now have $CuInSe_2$ precursor films that are free of sulfur and have reduced carbon impurities. Therefore, based on the current understanding of fine-grain layer formation, these precursor films have the potential to fully coarsen without fine-grain layer formation. To test this, the film was heated to 540 °C with selenium in a tube furnace. As shown in Figure 5b, the resulting film is fully coarsened, with no evidence of a fine-grain layer even with an absorber thicker than 2 μm. This result confirms recent hypotheses on fine-grain layer formation being connected to carbon impurities and the sulfide-to-selenide conversion.[14] Additionally, these methods open a path for solution-processed $CuInSe_2$ solar cells with an absorber layer thickness of 2 μm or more.

CONCLUSIONS

In this work, the soluble complexes obtained from amine−thiol dissolution were studied through a combination of Raman, XAS, ICP-OES, XRF, and ESI-MS/MS. While the amine−thiol solvent system has generally been used to make soluble metal thiolates that are useful in making metal sulfide films, we explored modifications to this system for the purpose of making metal selenides. We showed that by dissolving indium(III) selenide together with selenium and then isolating the complexes from the bulk thiol-containing solution, we can alter the soluble species. Raman and XAS analyses showed the presence of In−Se bonding in these isolated species. Compositional analysis with ICP-OES and XRF revealed that the thiols had been removed from the isolated complexes. ESI-MS/MS analysis showed the formation of soluble $[InSe_x]^-$ species. These methods were then translated to amine−thiol solutions of Cu_2Se + Se. Together, these soluble complexes provided an ink to fabricate solution-processed $CuInSe_2$ films that are free of sulfur. These sulfur-free $CuInSe_2$ precursor films were then coarsened into a 2 μm thick large-grain absorber layer that was free of any fine-grain layer, confirming that this fine-grain layer is connected to both carbon and sulfur in the precursor films.

ASSOCIATED CONTENT

Supporting Information

The Supporting Information is available free of charge at https://pubs.acs.org/doi/10.1021/acsomega.3c07515.

Additional XRD, ESI-MS/MS, Raman, and XRF data (PDF)

AUTHOR INFORMATION

Corresponding Author

Rakesh Agrawal − *Davidson School of Chemical Engineering, Purdue University, West Lafayette, Indiana 47907, United States;* orcid.org/0000-0002-6746-9829; Email: agrawalr@purdue.edu

Authors

Jonathan W. Turnley − *Davidson School of Chemical Engineering, Purdue University, West Lafayette, Indiana 47907, United States;* orcid.org/0000-0003-1262-6417

Swapnil D. Deshmukh − *Davidson School of Chemical Engineering, Purdue University, West Lafayette, Indiana 47907, United States;* orcid.org/0000-0001-7101-7393

Victoria M. Boulos − *Department of Chemistry, Purdue University, West Lafayette, Indiana 47907, United States*

Ryan G. Ellis − *Davidson School of Chemical Engineering, Purdue University, West Lafayette, Indiana 47907, United States;* orcid.org/0000-0002-6924-6936

Nicole J. LiBretto − *Davidson School of Chemical Engineering, Purdue University, West Lafayette, Indiana 47907, United States*

Judy Kuan-Yu Liu − *Department of Chemistry, Purdue University, West Lafayette, Indiana 47907, United States*

Jeffrey T. Miller − *Davidson School of Chemical Engineering, Purdue University, West Lafayette, Indiana 47907, United States;* orcid.org/0000-0002-6269-0620

Hilkka I. Kenttämaa − *Department of Chemistry, Purdue University, West Lafayette, Indiana 47907, United States;* orcid.org/0000-0001-8988-6984

Complete contact information is available at: https://pubs.acs.org/10.1021/acsomega.3c07515

Notes

The authors declare no competing financial interest.

ACKNOWLEDGMENTS

The authors thank the National Science Foundation for financial support through Grants 1735282-NRT (SFEWS) and 10001536 (INFEWS).

REFERENCES

(1) Nakamura, M.; Yamaguchi, K.; Kimoto, Y.; Yasaki, Y.; Kato, T.; Sugimoto, H. Cd-Free Cu(In,Ga)$(Se,S)_2$ Thin-Film Solar Cell with Record Efficiency of 23.35%. *IEEE J. Photovoltaics* **2019**, *9* (6), 1863−1867.

(2) Feurer, T.; Carron, R.; Sevilla, G. T.; Fu, F.; Pisoni, S.; Romanyuk, Y. E.; Buecheler, S.; Tiwari, A. N. Efficiency Improvement of Near-Stoichiometric $CuInSe_2$ Solar Cells for Application in Tandem Devices. *Adv. Energy Mater.* **2019**, *9* (35), No. 1901428.

(3) Suresh, S.; Uhl, A. R. Present Status of Solution-Processing Routes for Cu(In,Ga)$(S,Se)_2$ Solar Cell Absorbers. *Adv. Energy Mater.* **2021**, *11* (14), No. 2003743.

(4) Mitzi, D. B. Solution-Processed Inorganic Semiconductors. *J. Mater. Chem.* **2004**, *14* (15), 2355−2365.

(5) Kemell, M.; Ritala, M.; Leskelä, M. Thin Film Deposition Methods for $CuInSe_2$ Solar Cells. *Crit. Rev. Solid State Mater. Sci.* **2005**, *30* (1), 1−31.

(6) Kato, T.; Wu, J.-L.; Hirai, Y.; Sugimoto, H.; Bermudez, V. Record Efficiency for Thin-Film Polycrystalline Solar Cells Up to 22.9% Achieved by Cs-Treated Cu(In,Ga)$(Se,S)_2$. *IEEE J. Photovoltaics* **2019**, *9* (1), 325−330.

(7) Guo, Q.; Ford, G. M.; Hillhouse, H. W.; Agrawal, R. Sulfide Nanocrystal Inks for Dense $Cu(In_{1-x}Ga_x)(S_{1-y}Se_y)_2$ Absorber Films and Their Photovoltaic Performance. *Nano Lett.* **2009**, *9* (8), 3060−3065.

(8) Mcleod, S.; Alruqobah, E.; Agrawal, R. Liquid Assisted Grain Growth in Solution Processed Cu(In,Ga)$(S,Se)_2$. *Sol. Energy Mater. Sol. Cells* **2019**, *195*, 12−23.

(9) Zhao, X.; Deshmukh, S. D.; Rokke, D. J.; Zhang, G.; Wu, Z.; Miller, J. T.; Agrawal, R. Investigating Chemistry of Metal Dissolution in Amine-Thiol Mixtures & Exploiting It towards Benign Ink Formulation for Metal Chalcogenide Thin Films. *Chem. Mater.* **2019**, *31* (15), 5674−5682.

(10) Uhl, A. R.; Katahara, J. K.; Hillhouse, H. W. Molecular-Ink Route to 13.0% Efficient Low-Bandgap Cu$In(S,Se)_2$ and 14.7%

https://doi.org/10.1021/acsomega.3c07515
ACS Omega 2023, 8, 47262−47270

Efficient Cu(In,Ga)$(S,Se)_2$ Solar Cells. *Energy Environ. Sci.* **2016**, *9* (1), 130−134.
(11) Yuan, S.; Wang, X.; Zhao, Y.; Chang, Q.; Xu, Z.; Kong, J.; Wu, S. Solution Processed Cu(In,Ga)$(S,Se)_2$ Solar Cells with 15.25% Efficiency by Surface Sulfurization. *ACS Appl. Energy Mater.* **2020**, *3*, 6785−6792.
(12) Clark, J. A.; Murray, A.; Lee, J.-M.; Autrey, T. S.; Collord, A. D.; Hillhouse, H. W. Complexation Chemistry in N,N-Dimethylformamide-Based Molecular Inks for Chalcogenide Semiconductors and Photovoltaic Devices. *J. Am. Chem. Soc.* **2019**, *141*, 298−308.
(13) Ellis, R. G.; Turnley, J. W.; Rokke, D. J.; Fields, J. P.; Alruqobah, E. H.; Deshmukh, S. D.; Kisslinger, K.; Agrawal, R. Hybrid Ligand Exchange of Cu(In,Ga)S_2 Nanoparticles for Carbon Impurity Removal in Solution-Processed Photovoltaics. *Chem. Mater.* **2020**, *32*, 5091−5103.
(14) Deshmukh, S. D.; Weideman, K. G.; Ellis, R. G.; Kisslinger, K.; Agrawal, R. Enabling Fine-Grain Free 2-Micron Thick CISe/CIGSe Film Fabrication via a Non-Hydrazine Based Solution Processing Route. *Mater. Adv.* **2022**, *3* (7), 3293−3302.
(15) Guo, Q.; Kim, S. J.; Kar, M.; Shafarman, W. N.; Birkmire, R. W.; Stach, E. A.; Agrawal, R.; Hillhouse, H. W. Development of $CuInSe_2$ Nanocrystal and Nanoring Inks for Low-Cost Solar Cells. *Nano Lett.* **2008**, *8* (9), 2982−2987.
(16) Ellis, R. G.; Deshmukh, S. D.; Turnley, J. W.; Sutandar, D. S.; Fields, J. P.; Agrawal, R. Direct Synthesis of Sulfide-Capped Nanoparticles for Carbon-Free Solution-Processed Photovoltaics. *ACS Appl. Nano Mater.* **2021**, *4*, 11466−11472.
(17) Sharma, R. K.; Kedarnath, G.; Kushwah, N.; Pal, M. K.; Wadawale, A.; Vishwanadh, B.; Paul, B.; Jain, V. K. Indium(III) (3-Methyl-2-Pyridyl)Selenolate: Synthesis, Structure and Its Utility as a Single Source Precursor for the Preparation of In_2Se_3 Nanocrystals and a Dual Source Precursor with $[Cu\{SeC_5H_3(Me\text{-}3)N\}]_4$ for the Preparation of $CuInSe_2$. *J. Organomet. Chem.* **2013**, *747*, 113−118.
(18) Pal, M. K.; Dey, S.; Neogy, S.; Kumar, M. Synthesis and Structure of $[(Ph_3P)_2Cu(\mu\text{-}SeCH_2Ph)_2In(SeCH_2Ph)_2]$ as a Single-Source Precursor for the Preparation of $CuInSe_2$ Nano-Materials. *RSC Adv.* **2019**, *9*, 18302−18307.
(19) Dhingra, S.; Kanatzidis, M. G. The Use of Soluble Metal-Polyselenide Complexes As Precursors to Binary and Ternary Solid Metal Selenides. *Mater. Res. Soc. Symp. Proc.* **1990**, *180*, 825−830.
(20) Norako, M. E.; Brutchey, R. L. Synthesis of Metastable Wurtzite $CuInSe_2$ Nanocrystals. *Chem. Mater.* **2010**, *22* (5), 1613−1615.
(21) Tappan, B. A.; Barim, G.; Kwok, J. C.; Brutchey, R. L. Utilizing Diselenide Precursors toward Rationally Controlled Synthesis of Metastable $CuInSe_2$ Nanocrystals. *Chem. Mater.* **2018**, *30* (16), 5704−5713.
(22) Agrawal, R.; Walker, B. C. Homogeneous Mixtures for Nanoparticle Synthesis. U.S. Patent US9,630,845 B2, 2017.
(23) Zhang, R.; Cho, S.; Lim, D. G.; Hu, X.; Stach, E. A.; Handwerker, C. A.; Agrawal, R. Metal−Metal Chalcogenide Molecular Precursors to Binary, Ternary, and Quaternary Metal Chalcogenide Thin Films for Electronic Devices. *Chem. Commun.* **2016**, *52* (28), 5007−5010.
(24) McCarthy, C. L.; Brutchey, R. L. Solution Processing of Chalcogenide Materials Using Thiol-Amine "'alkahest'" Solvent Systems. *Chem. Commun.* **2017**, *53*, 4888.
(25) Webber, D. H.; Buckley, J. J.; Antunez, P. D.; Brutchey, R. L. Facile Dissolution of Selenium and Tellurium in a Thiol-Amine Solvent Mixture under Ambient Conditions. *Chem. Sci.* **2014**, *5*, 2498.
(26) Lin, Z.; He, Q.; Yin, A.; Xu, Y.; Wang, C.; Ding, M.; Cheng, H.-C.; Papandrea, B.; Huang, Y.; Duan, X. Cosolvent Approach for Solution-Processable Electronic Thin Films. *ACS Nano* **2015**, *9* (4), 4398−4405.
(27) Deshmukh, S. D.; Ellis, R. G.; Sutandar, D. S.; Rokke, D. J.; Agrawal, R. Versatile Colloidal Syntheses of Metal Chalcogenide Nanoparticles from Elemental Precursors Using Amine-Thiol Chemistry. *Chem. Mater.* **2019**, *31* (21), 9087−9097.
(28) Walker, B. C.; Agrawal, R. Contamination-Free Solutions of Selenium in Amines for Nanoparticle Synthesis. *Chem. Commun.* **2014**, *50*, 8331−8334.
(29) Deshmukh, S. D.; Easterling, L. F.; Manheim, J. M.; Libretto, N. J.; Weideman, K. G.; Miller, J. T.; Kenttämaa, H. I.; Agrawal, R. Analyzing and Tuning the Chalcogen−Amine−Thiol Complexes for Tailoring of Chalcogenide Syntheses. *Inorg. Chem.* **2020**, *59* (12), 8240−8250.
(30) Kärber, E.; Otto, K.; Katerski, A.; Mere, A.; Krunks, M. Raman Spectroscopic Study of In_2S_3 Films Prepared by Spray Pyrolysis. *Mater. Sci. Semicond. Process.* **2014**, *25*, 137−142.
(31) Chung, C.-H.; Li, S.-H.; Lei, B.; Yang, W.; Hou, W. W.; Bob, B.; Yang, Y. Identification of the Molecular Precursors for Hydrazine Solution Processed $CuIn(Se,S)_2$ Films and Their Interactions. *Chem. Mater.* **2011**, *23*, 964−969.
(32) Zhou, H.; Hsu, C.-J.; Hsu, W.-C.; Duan, H.-S.; Chung, C.-H.; Yang, W.; Yang, Y.; Zhou, H. P.; Hsu, C.; Hsu, W.; et al. Non-Hydrazine Solutions in Processing $CuIn(S,Se)_2$ Photovoltaic Devices from Hydrazinium Precursors. *Adv. Energy Mater.* **2013**, *3*, 328−336.
(33) Murria, P.; Miskin, C. K.; Boyne, R.; Cain, L. T.; Yerabolu, R.; Zhang, R.; Wegener, E. C.; Miller, J. T.; Kenttämaa, H. I.; Agrawal, R. Speciation of CuCl and $CuCl_2$ Thiol-Amine Solutions and Characterization of Resulting Films: Implications for Semiconductor Device Fabrication. *Inorg. Chem.* **2017**, *56* (23), 14396−14407.
(34) Kanatzidis, M. G.; Huang, S. P. Coordination Chemistry of Heavy Polychalcogenide Ligands. *Coord. Chem. Rev.* **1994**, *130*, 509−621.
(35) Dhingra, S. S.; Kanatzidis, M. G. Polyselenide Chemistry of Indium and Thallium in Dimethylformamide, Acetonitrile, and Water. Syntheses, Structures, and Properties of the New Complexes $[In_2(Se_4)_4(Se_5)]^{4-}$, $[In_2Se_2(Se_4)_2]^{2-}$, $[In_3Se_3(Se_4)_3]^{3-}$, and $[Tl_3Se_3(Se_4)_3]^{3-}$. *Inorg. Chem.* **1993**, *32*, 1350−1362.
(36) Kanatzidis, M. G. Soluble Polychalcogenides of the Late Transition and Main Group Elements. *Comments Inorg. Chem.* **1990**, *10*, 161−195.
(37) Schmid, T.; Schäfer, N.; Levcenko, S.; Rissom, T.; Abou-Ras, D. Orientation-Distribution Mapping of Polycrystalline Materials by Raman Microspectroscopy. *Sci. Rep.* **2016**, *5*, No. 18410.
(38) Oja, I.; Nanu, M.; Katerski, A.; Krunks, M.; Mere, A.; Raudoja, J.; Goossens, A. Crystal Quality Studies of $CuInS_2$ Films Prepared by Spray Pyrolysis. *Thin Solid Films* **2005**, *480−481*, 82−86.
(39) Dzhagan, V.; Litvinchuk, A. P.; Ya Valakh, M.; T Zahn, D. R. Phonon Raman Spectroscopy of Nanocrystalline Multinary Chalcogenides as a Probe of Complex Lattice Structures. *J. Phys.: Condens. Matter* **2023**, *35*, No. 103001.
(40) Xu, C.-M.; Xu, X.-L.; Xu, J.; Yang, X.-J.; Zuo, J.; Kong, N.; Huang, W.-H.; Liu, H.-T. Composition Dependence of the Raman A_1 Mode and Additional Mode in Tetragonal Cu−In−Se Thin Films. *Semicond. Sci. Technol.* **2004**, *19*, 1201−1206.
(41) Fonoll-Rubio, R.; Paetel, S.; Grau-Luque, E.; Becerril-Romero, I.; Mayer, R.; Pérez-Rodríguez, A.; Guc, M.; Izquierdo-Roca, V. Insights into the Effects of RbF-Post-Deposition Treatments on the Absorber Surface of High Efficiency Cu(In,Ga)Se_2 Solar Cells and Development of Analytical and Machine Learning Process Monitoring Methodologies Based on Combinatorial Analysis. *Adv. Energy Mater.* **2022**, *12*, No. 2103163.
(42) Chu, P. K.; Li, L. Characterization of Amorphous and Nanocrystalline Carbon Films. *Mater. Chem. Phys.* **2006**, *96*, 253−277.
(43) Todorov, T. K.; Hillhouse, H. W.; Aazou, S.; Sekkat, Z.; Vigil-Galán, O.; Deshmukh, S. D.; Agrawal, R.; Bourdais, S.; Valdés, M.; Arnou, P.; et al. Solution-Based Synthesis of Kesterite Thin Film Semiconductors. *J. Phys. Energy* **2020**, *2*, No. 012003.
(44) Ramanathan, K.; Bhattacharya, R.; Contreras, M.; Keane, J. C.; To, B.; Dhere, R. G.; Noufi, R. *High Performance CIGS Thin Film Solar Cells: A Laboratory Perspective*; NREL: 2005.

https://doi.org/10.1021/acsomega.3c07515
ACS Omega 2023, 8, 47262−47270